ACS APPLIED MATERIALS & INTERFACES

Research Article

www.acsami.org

Study of Wetting on Chemically Soften Interfaces by Using Combined Solution Thermodynamics and DFT Calculations: Forecasting Effective Softening Elements

Guo Gang Shu,[†] Qiang Xu,[‡] and Ping Wu*[,‡]

[†]Nuclear Materials Joint Lab, Tsinghua University Graduate School, Tsinghua University City Park, Shenzhen 518055, China

[‡]Entropic Interface Group, Engineering Product Development, Singapore University of Technology and Design, 8 Somapah Road, Singapore 487372, Singapore

Supporting Information

ABSTRACT: Despite recent progress in understanding the wetting principles on soft solids, the roles of chemical bonding in the formation of interfaces have been largely ignored, because most of these studies are conducted at room temperatures. Here we propose a universal wetting principle from solution thermodynamics to account for the softening of both the solid and liquid surfaces (stable or metastable). Density functional theory (DFT) calculations are applied to evaluate the stability and electron transportation across the interfaces. We find that wetting is dominated by the system entropy changes involving not only the stable liquid alloy phase but also the metastable liquid oxide phases. The state-of-art multicomponent solution thermodynamic models and databases are applied to describe the entropy changes and predict the wetting behaviors. Our results show that by chemically softening either the liquid or the solid phase, the wetting angle reduces. And an effective soften agent/additive (either in the form of chemical elements or molecules) will weaken the bonds within the liquid (or solid) phase and promote new bonds at the interfaces, thus increasing the interface entropy. Subsequently, as an example, Ti and Zr are proposed as effective softening elements to improve the wetting of aluminum liquid on B_6Si(s). This approach provides a concept and tool to advance research in catalytic chemistry, nucleation (growth), elastowetting, and cell−substrate interactions.

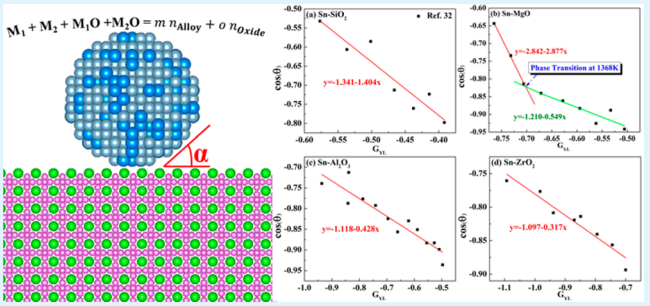

KEYWORDS: *wetting, soften interfaces, thermodynamics, chemical bonding, electronic structures, density functional theory*

1. INTRODUCTION

The process of wetting for a liquid on a soft and deformable material surface has been intensively investigated over the past half century.[1−19] A recent breakthrough[1,2,20] allows detailed observation of the wetting ridge geometry where gas, liquid and solid phases joint. Park et al.[1] found a strong correlation between the solid Young's modulus and the area of the liquid/solid interface; solid with higher Young's modulus prefers a reduce liquid/solid interface area. Because Young's modulus is a measure of the bond stiffness (normalized by bond length), it is expected that chemical bonding plays a crucial role in determining the wetting ridge geometry. However, influence of chemical bonding to the wetting on soft materials has so far been largely ignored, due to the characteristic secondary bonding in soft materials. On the other hand, the role of chemical bonding in the wetting of solid by liquid alloys is well-known.[21,22] At an early nucleation and growth stage, the interface is soft in comparison with the fully grown solid, due to the formation of metastable-amorphous-like interface structures that have much lower Young's modulus. The solid surface is then softened by the adjacent liquid atoms through a bond breaking and/or formation process, similar to a recent report[23] on the two-step nucleation in solid−solid transition involving liquid nuclei.

We shall look into thermodynamic principles that govern the early stage of wetting with a chemically softened solid surface, involving both stable and metastable phases.[23] Many efforts are reported in developing thermodynamic theory and models for liquid/solid interfaces. Naidich[24,25] estimated the bonding energy between liquid alloy and solid oxide using a redox reaction energy and tried to explain the observed wetting behaviors. But partially by the lack of quality thermodynamic models and databases, especially for liquid solutions at the time, no clear thermodynamic property or calculation protocol was established that predicts the wetting behaviors. In this work, by applying the state-of-art solution thermodynamic models and databases together with density functional theory (DFT) calculations, we propose a principle and method for the study of wetting on chemically softened solid surfaces.

Received: December 21, 2014
Accepted: March 25, 2015
Published: April 6, 2015

DOI: 10.1021/am509013m
ACS Appl. Mater. Interfaces 2015, 7, 7576−7583

Although wetting is not strictly an isobaric nor isometric process, reaction Gibbs free energy or Helmholtz free energy is often used to simulate the system energy changes. It is not a surprise that most of the thermodynamic analysis for interfaces starts from the work of adhesion, which is the change in interface energy due to the destruction of old (liquid/solid) and the formation of two new interfaces (liquid/vapor and solid/vapor). And, it is well documented that cosine wetting angle can be calculated from the work of adhesion and the vapor/liquid interface energy.[26] To derive a more general principle and practical method for the wetting study, we start from the second law of thermodynamics, which states that there is an increase (during the wetting process) in the sum of the entropies of the vapor−liquid−solid three-phase system. It is of interest that the role of entropy in phase (or ordering) transition has attracted increasing attention recently.[27,28]

In our three-phase-system, the gas phase has the largest entropy among all three phases and is expected to dominate the changes in the system entropy; we then first revisit the Young−Laplace equation,[29] which indicates that the surface radius of a vapor bubble is inversely proportional to the pressure drop when the surface expands, hence the wetting angle (or wetting joint geometry) is associated with the surface pressure drops. For a general wetting process where a liquid metal (M_1) is in contact with a solid oxide (M_2O), the surface pressure drops is further linked to the evolution of oxygen partial pressures in the $M_1 + M_2 + M_1O + M_2O$ system. On the other hand, the entropy of mixing for an *n*-mole two component (1 and 2) ideal solution is $\Delta S_{mix} = -nR\,(x_1 \ln x_1 + x_2 \ln x_2)$, where R is the gas constant and x_i the mole fraction of component i. In an idea gas phase, the partial pressure of component i equals the mole fraction of i; $P_i = x_i$. Therefore, the wetting angle may be determined by the entropy changes, which are functions of oxygen partial pressures and/or constituent molar fractions of both the liquid alloy and the metastable liquid oxide phases[23] in the following redox reaction:

$$M_1 + M_2 + M_1O + M_2O = mn_{Alloy} + on_{Oxide} \quad (1)$$

where a mixture of 1 mol of M_1, 1 mol of M_2, 1 mol of M_1O and 1 mol of M_2O reacts to form *m* moles of liquid metal alloy n_{Alloy} and *o* moles of metastable liquid oxide n_{Oxide}.[30,31] n_{Alloy} and n_{Oxide} are respectively a binary solution (M_1−M_2 for Alloy and M_1O−M_2O for Oxide). Equation 1 is the formation reaction of two binary solutions (alloy and oxide) from two unary metals and two unary oxides, which represents the formation of alloy/oxide interfaces during wetting.

We shall demonstrate how to apply eq 1 by four industrial case studies. In case 1, only one metal (M_1 = Sn) wets on one oxide (M_2O = SiO_2, MgO, Al_2O_3, or ZrO_2, respectively), and the formed alloy or oxide based on eq 1 is a pure Sn for n_{Alloy} and SiO_2, MgO, Al_2O_3, or ZrO_2 for n_{Oxide}. Because both the activity of Sn in liquid and the activity of the metal oxide in solid are in unity, it is sufficient to represent the entropy changes and thus approximate wetting angles by oxygen partial pressures of eq 1. In case 2, a zinc-alloy wets on a steel surface to form initially a multicomponent alloy and oxide phases as in eq 1. The alloy and oxide are no longer single components, as in case 1, but solutions. Entropy changes brought up by gas phase (via oxygen partial pressure) and the other two phases (via the formation of multicomponent alloy and oxide) can be approximated by a chemical equilibrium calculation on eq 1. The entropy changes after partitioning nx_2 moles of M_1 from the n_{Alloy} (which initially is a unary phase) to the n_{Oxide} solution can be estimated by the partition-configuration-entropy of M_1: $\Delta S_{mix} = -nR\,(x_1 \ln x_1 + x_2 \ln x_2)$, where x_1 and x_2 (=1 − x_1) are the molar fractions of M_1 left in the alloy and the oxide phase, respectively. Therefore, the partition of each constituent among difference phases, or the configuration entropy of a constituent, may be used as a rough indicator for changes in system entropy. Using the resultant phase partitions (between alloy and oxide) of each constituents, which are functions of entropy changes, we explain well the experiment observations in zinc galvanizing, and subsequently we reveal the thermodynamics basis that favors lower wetting angles (i.e., increase in entropy). In case 3, an Al-alloy wets on the B_4C substrate. By eq 1, the formed Al-alloy and the Al_2O_3-containing oxide (a metastable phase appeared at the early stage of wetting) are multicomponent phases. Similar to case 2, our calculations agree well with the observed Al/B_4C wetting experiments. Finally, in case 4, we predict the wetting of Al-alloy on the B_6Si substrate using eq 1. Becuase there is no experiment reported so far and furthermore both DFT and MD calculations simulated well the Al/AlB_2 interfaces,[32,33] DFT calculations are used to verify the model developed by thermodynamic calculations based on eq 1. And good agreements are reached between the two models with regards to the physics of the wetting at the atomic/electronic levels. For each of the four cases more details will be given below, however, the final results will be reported in the later sections.

Case 1: Wetting of Sn on Each of SiO_2, MgO, Al_2O_3, and ZrO_2. The n_{Alloy} and n_{Oxide} in eq 1 become a pure metal Sn and one of the above four single oxides, respectively. Entropy changes during wetting are dominated by the gas phase. We approximate the entropy changes by changes in oxygen partial pressures, which can also be readily read from the Ellingham diagram. In the last century, abundant knowledge and tools have been devoted to the thermodynamics in gas-pure metal-pure oxide systems, driven mainly by metal extraction practice. In particular, the difference in oxygen partial pressures ($_1PO_2$ and $_2PO_2$) for two metals (M_1 and M_2), which is associated with the surface pressure drops, can be directly read from the so-called Ellingham diagram[34] at any given temperature, where $_1PO_2$ and $_2PO_2$ are, respectively, the reaction oxygen partial pressure:

$$M_1 + 0.5O_2 = M_1O \quad (2)$$

and

$$M_2 + 0.5O_2 = M_2O \quad (3)$$

Alternatively, the difference of $_1PO_2$ and $_2PO_2$ in logarithm form at a given temperature can be calculated from the reaction energy (ΔG_3):

$$0.5M_1 + 0.5M_2O = 0.5M_2 + 0.5M_1O \quad (4)$$

For example, from the Ellingham diagram,[35] $(4.0 \times 10^{-21})^{1/2}$ (−377.0/2 kJ/mol), $(1.0 \times 10^{-36})^{1/2}$ (−715.0/2 kJ/mol), and 398.0/2 kJ/mol are, respectively, the oxygen partial pressure (Gibbs energy of formation) of SnO_2 in eq 2, of SiO_2 in eq 3, and the reaction Gibbs energy of eq 4 at 727 °C, where the simple operations are taken because the reactions in the Ellingham diagram are based on per mol O_2, whereas eq 4 is based on per mol of metal).

Assume M_1, M_2O, and oxygen-containing gas are in liquid, solid, and vapor phase, respectively, eq 4 simulates the chemical reactions during the wetting of liquid metal (M_1) on a solid oxide (M_2O), and the reaction energy mimics the work of

DOI: 10.1021/am509013m
ACS Appl. Mater. Interfaces 2015, 7, 7576−7583

adhesion. Therefore, the pressure drops and work of adhesion can be simulated by using eq 4 and can be visualized using the Ellingham diagram (as the example shown above). Practically, eqs 1 and 4 are just two different ways of presenting the redox reactions between Sn and the oxide. We further apply the normalized formation energy difference $G_{YL} = (\Delta G_1 - \Delta G_2)/\Delta G_1 = \ln({}_2PO_2/{}_1PO_2)/\ln{}_1PO_2$ for eq 4 to represent the relative pressure drops (term) defined in the Young Laplace equation. ΔG_1 and ΔG_2 are, respectively, the Gibbs free energies of reactions 2 and 3, and both ${}_2PO_2$ and ${}_1PO_2$ can be read from the Ellingham diagram (as shown above). In a more general form, eq 4 can be rewritten as

$$M_1^{\circ} + M_2^{+n} = M_2^{\circ} + M_1^{+m} + (m - n)e \quad (5)$$

where n and m are the charges of the M_2 and M_1 cation, respectively. Because the vapor phase contributes to the largest portion of the total entropy changes, we calculate (or read from the Ellingham diagram) G_{YL} and use it to explain the reported wetting behaviors in the four vapor phase dominant systems; Sn-M_iO (i = SiO_2, MgO, Al_2O_3, and ZrO_2), where entropy varies with temperature only.

Case 2: Wetting of Zn on Steel. We further extend the above calculations to systems containing alloys of higher melting temperatures and nonoxides, where entropy changes in liquid are no longer ignorable. Using eq 1, we approximate the entropy changes from the partition of metallic elements between the stable liquid alloy and metastable liquid oxide phases. And we explain well the softening (by alloying) of the liquid surface in zinc galvanizing at 450 °C. Our models are consistent with experiment reports.

Case 3: Wetting of Al on B_4C. In this system, the entropy is still dominated by the gas phase and the entropy changes of the liquid alloys (having even higher melting temperatures) are no longer ignorable. Using eq 1 we approximate the entropy changes from the partition of metallic elements between the stable liquid alloy and metastable liquid oxide phases. Our thermodynamic calculations on eq 1 reproduce well the reported experiment observations about Ti-alloying.

Case 4: Wetting of Al on B_6Si. Furthermore, on the basis of eq 1, we predict new effective softening elements (Ti and Zr) in the Al−B_6Si system, which demonstrated the forecasting power of this general model.

Therefore, this study provides an opportunity not only to advance the fundamental understanding on wetting process but also to develop a practical tool in the design/development of new additives to control the nucleation and growth process at interfaces.

2. SOLUTION THERMODYNAMICS AND DFT CALCUALTIONS

All thermodynamic calculations in this study are conducted by using the FactSage[36] computing system. We typically (1) insert the reactants of eq 1 into the Equilib module of the software; for example, we input 1 mol of metals (M_1) and 1 mol of its metal oxide (like M_1O) for all metals involved in the Zn-galvanizing process, (2) select two phases (a stable liquid alloy and a metastable liquid slag (or oxide solution)) from the FactSage solution database list, (3) setup the wetting temperature, (4) conduct energy minimization for the system to reach equilibrium, and (5) read the output file, which shows the equilibrium amount of the two phases as well as the constituent molar fractions of each phase. More details on the case study for Zn-galvanizing will be given when eq 6 is introduced.

All DFT calculations are carried out using the all-electron-like projector augmented wave (PAW) method[37] and the Perdew−Burke−Ernserhof (PBE) exchange correlation potential[38] as implemented in the Vienna Ab-initio Simulation Package (VASP).[39] We applied DFT calculations to further confirm the stability as well as the expected electron transportation across the interface between Al and B_6Si. For the DFT calculations, the cutoff energy for the plane wave expansion of the wave functions is 500 eV, and the Hellman−Feynman forces are less than 5 meV/Å. The lattice parameters of B_3Si, B_6Si and Al are fully optimized, which the sufficient k-points of Monkhorst−Pack grids[40] for Brillouin zone integration were taken in order to make the calculations of relaxation converge. For the calculations of B_3Si/Al and B_6Si/Al interfaces, the superlattices of B_3Si/Al and B_6Si/Al are built with (B_3Si 1 × 1 × 2 supercell)/(Al 2 × 3 × 3 supercell), and (B_6Si 1 × 1 × 4 supercell)/(Al 1 × 1 × 4 supercell), respectively. All interfaces are along the (0 0 1) direction. The optimized lattice parameters in x−y plane of B_3Si and B_6Si are taken as the corresponding lattice parameters of B_3Si/Al and B_6Si/Al superlattices, respectively. All ions in superlattices are fully relaxed. The Brillouin zone integration of the superlattice of B_3Si/Al and B_6Si/Al is performed using 4 × 2 × 1 and 8 × 8 × 1 Monkhorst−Pack grids. For the calculations of the B_6Si/Al interface doped with Cu, Ti, and Zr substituting the Al site, the superlattice of $B_6Si(2 \times 2 \times 4)$/Al$(2 \times 2 \times 4)$ is employed. The details of the DFT models are listed in the Supporting Information.

3. RESULTS AND DISCUSSION

We shall first report how to reproduce the measured wetting to temperature dependence by using a single thermodynamic property, G_{YL}, which can also be read from the Ellingham diagram, in four pure tin/oxide systems. Then extend the wetting calculation to include alloys and nonoxides; finally, we apply the developed principle and calculation method to predict new additives for aluminum wetting on B_6Si substrate.

3.1. Wetting of Pure Liquid Tin on Solid Surfaces in Each of the Four Sn−M_iO (i = SiO_2, MgO, Al_2O_3, and ZrO_2) Systems. As shown in Figure 1, K. Nogi et al.[41] measured the wetting angles of pure liquid tin on solid oxides (SiO_2, MgO, Al_2O_3, and ZrO_2) by the sessile drop method. They found that the wetting angles are linearly correlated to the wetting temperatures. We calculated G_{YL} for each of their experiment points in the four systems, and obtained a direct linear relationship between the cosine of wetting angle and G_{YL}, as shown in Figure 1a (Sn−SiO_2), Figure 1b (Sn−MgO),

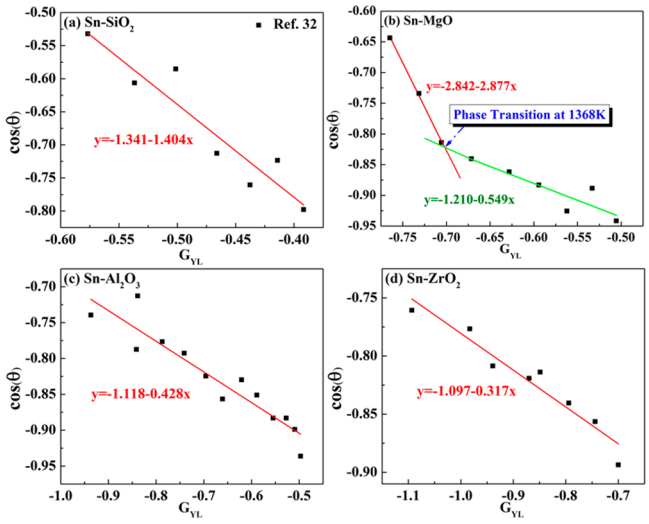

Figure 1. Linear relationship between experiment[32] (cosine wetting angles) and calculated G_{YL}, in Sn−SiO_2, −MgO, −Al_2O_3, and −ZrO_2 systems. The formulas listed in panels a−d are obtained by using the least-squares regression method.

DOI: 10.1021/am509013m
ACS Appl. Mater. Interfaces 2015, 7, 7576−7583

Figure 1c (Sn−Al_2O_3), and Figure 1d (Sn-ZrO_2), at a temperature range of 700−1700 K. It is interesting that the effect of Mg phase transition (from liquid to gas at 1368 K) automatically accounts for in the G_{YL} calculations, as demonstrated in Figure 1b where the two lines join between the two experiment points (1308 and 1403 K) that are the closest in temperature to 1368 K. Because G_{YL} represents the pressure drops (with reference to the oxygen partial pressure at the gas/liquid metal interface) across the gas/liquid metal and gas/solid oxide interfaces, and the pressure drops are associated with the dominating gas phase entropy changes, it is no surprise that we can establish a linear relationship between the cosine of wetting angles and G_{YL}. It seems that the higher the absolute value of G_{YL} (or the larger the relative pressure drop), the smaller the wetting angle. This is expected because an increase in gas phase entropy stabilizes the gas/liquid metal/solid oxide system. To demonstrate the prediction power of the regression equation in Figure 1a, here we calculate the cosine of wetting angle at 1000 K, which was reported as −0.65 by K. Nogi et al.[41] By using $G_{YL} = (\Delta G_1 - \Delta G_2)/\Delta G_1 = (-367\ 522\ \text{J/mol} + 730\ 288\ \text{J/mol})/(-367\ 522\ \text{J/mol}) = -0.50$, and the regression equation in Figure 1a, our predicted cosine wetting angle is −0.64, which is very close to the experiment value of −0.65. Alternatively, we can read the oxygen partial pressures from the Ellingham diagram (as shown earlier) and use $G_{YL} = \ln({}_2PO_2/{}_1PO_2)/\ln {}_1PO_2$ to reach the same result.

3.2. Softening of Liquid Surface in Zinc Galvanizing-Extension from the Wetting of Pure Liquid Metals to Liquid Alloys. Although the vapor phase contributes to the largest entropy changes of the system, we still have to account for the entropy changes in the liquid and solid phases if they do not remain constant in the studied systems. In zinc galvanizing, minor metallic element/additives are commonly applied into the molten zinc to improve the quality of the coating formation. Addition of 0.1 wt % Ni will reduce the coating thickness by about 3-fold,[21,22] but no improvement is reported with Cu addition. The effect of chemical additives (Ni, Ti, and Zr) on the steel weight loss was measured by Sebisty et al.[42] in the galvanizing of rimmed steel at 460 °C. They reported that without any additive the original steel weight loss was 27.8 g/m^2. But by adding 0.2% Ni the observed weight loss was reduced to 22.3 g/m^2, and the wetting angle of Zn on steel reduces. To calculate the above wetting behaviors, we have to take into consideration the changes in liquid entropy that is no longer ignorable. By solution thermodynamic calculations, we confirm that Ni, not Cu, is an effective liquid phase softening element. A general design principle for the selection of alloy elements in the zinc galvanizing process is subsequently developed.

We first check if a Ni−Zn liquid solution is positively or negatively deviated from an ideal solution, which will indicate if the Ni−Zn atomic bonding is promoted. The calculated activity coefficients of Zn and Ni, at 450 °C in the Zn−Ni liquid phase at a composition of equal molar ratio, are 1.01 and 1.50, respectively, from FactSage, which indicates that this Ni−Zn alloy is positively deviated from an ideal solution. Therefore, by adding Ni into molten Zn, the liquid phase becomes less stable (or soften), and the added Ni atoms will be repelled away from the liquid zinc phase and mobile to the surface. Similarly, the calculated activity coefficients of Zn and Cu at 450 °C are 0.276 and 0.280, respectively, which confirms that Cu−Zn is a negative deviated solution. Cu atoms form strong Cu−Zn bonds in the liquid (or hardening) and destabilize the Zn/ZnO interface, which results in larger wetting angles than in the pure zinc wetting. The above solution thermodynamic calculations explain well the experiment observations. To demonstrate further the thermodynamic competition between Ni and Cu additions, we simulate their softening effects to the gas/M_1 (liquid) interfaces (in eq 4) by an equilibrium calculation of eq 1 at 450 °C of two phases; one liquid alloy (1 mol of Zn, 1 mol of Ni, and 1 mol of Cu) and one liquid oxide (ZnO + NiO + Cu_2O), as shown below:

$$\text{Zn} + \text{Ni} + \text{Cu} + \text{ZnO} + \text{NiO} + \text{Cu}_2\text{O} = 3.99n^{\text{I}}_{\text{Alloy}} + 3.00n^{\text{I}}_{\text{Oxide}} \quad (6)$$

where the molar fractions of liquid alloy $n^{\text{I}}_{\text{Alloy}}$ are 0.75 Cu, 0.25 Ni, and 8.0×10^{-6} Zn, and the molar fractions of liquid oxide $n^{\text{I}}_{\text{Oxide}}$ are 0.67 ZnO, 0.33 NiO, and 4.0×10^{-3} Cu_2O.

Before wetting, the system initially consists of 1 mol of Zn, 1 mol of Ni, and 1 mol of Cu for the alloy and 1 of mol ZnO, 1 mol of NiO, and 1 mol of Cu_2O for the oxide, After equilibrium is reached between the alloy and the oxide phase, there are 3.99 mol of alloy and 3.00 mol oxide formed (based on FactSage calculations). And the calculated partition-configuration-entropy values of Cu and Ni are, respectively, 2.9 and 4.7 J K^{-1} mol^{-1}. Almost all Cu atoms are concentrated in the liquid alloy phase and rarely in the oxide phase, but the opposite trend is seen for Ni, which results in the higher partition-configuration-entropy. Although the final real oxide product is a solid, we use the thermodynamic model for liquid oxide solutions to mimic the interface with the amorphous-like oxides at the early nucleation stage.

The pressure drop at the vapor/liquid interface is the driving force in determining the wetting joint geometry. When the change in entropy contributed from either the liquid or the solid phase is no longer invariant, these entropy changes have to be calculated by using the state-of-art of solution chemistry models and databases. Alloy elements are predicted to improve the wetting if they have lower partition in the liquid metal (via forming positive deviated solution or softening the liquid) than in the amorphous oxide phase.

3.3. Softening of Liquid Surface in Al−B_4C System-Extension from the Wetting on Oxides to Nonoxide Substrates. Aluminum is strengthened by forming a metal matrix composite (MMC) with B_4C for commercial applications like lightweight rails for high speed trains and neutron absorbents in nuclear power plants. The effect of chemical additives (Ti and Zr) on the wetting of B_4C was measured by Oh et al.[43] using pressure infiltration of liquid Al alloys into the B_4C powder specimens at a temperature range of 700−900 °C. Therefore, Ti alloying in Al may improve wetting but no improvement was observed for Cu alloying.[43,44] To explain the above wetting behaviors, we have to expand our solution thermodynamic calculations (on eq 1) to include nonoxide like B_4C.

Although there it is a reactive interface, the initial nucleation mechanism of Al rich clusters on the B_4C surface is modulated by the solution chemistry of the MMC. This expansion of the method (eq 1) to nonoxide systems makes it possible to study new wetting theory on 2D structures like CNT[45] and BNNT[46] in the future.

We first calculate the solid oxidation sequence in the Al−B_4C system by reacting 1 mol of Al and 1 mol of B_4C with n mol of O_2 at 750 °C, using FactSage software. The results indicate that Al_2O_3 and $(Al_2O_3)_9(B_2O_3)$ start to form, respectively, at n <

DOI: 10.1021/am509013m
ACS Appl. Mater. Interfaces 2015, 7, 7576−7583

0.001 and n = 0.60. Therefore, the oxidation sequence at the Al/B_4C interface is Al^{3+} and followed by B^{3+}, which means Al_2O_3 and B_2O_3 may participate in the early nucleation stage at the Al/B_4C interface. To demonstrate the thermodynamic competition between Ti and Cu additions in the Al−B_4C system, we simulate their softening effects at the gas/Al (liquid) interfaces by a modified eq 1; an equilibrium calculation at 750 °C of two phases; one liquid alloy (Al + Ti + Cu) plus one liquid oxide (Al_2O_3 + B_2O_3+ TiO_2 + Cu_2O), as shown below:

$$\mathrm{Al} + \mathrm{Ti} + \mathrm{Cu} + \mathrm{Al_2O_3} + \mathrm{TiO_2} + \mathrm{Cu_2O} + \mathrm{B_2O_3} = 4.00 n^{\mathrm{II}}_{\mathrm{Alloy}} + 3.00 n^{\mathrm{II}}_{\mathrm{Oxide}} \quad (7)$$

where the molar fractions of liquid alloy $n^{\mathrm{II}}_{\mathrm{Alloy}}$ are 0.13 Al, 0.75 Cu, and 0.11 Ti, the molar fractions of liquid oxide n^{II}_{Oxide} are 0.41 Al_2O_3, 0.25 Ti_2O_3, 2.7 × 10^{-3} TiO_2, 6.3 × 10^{-9} Cu_2O, and 0.33 B_2O_3. The calculated partition-configuration-entropy values of Cu and Ti are, respectively, 2.9 and 4.2 J K^{-1} mol^{-1}. It is clear that Cu and Ti atoms enriched respectively in the alloy and oxide phase. Therefore, Ti atoms prefer moving away from the liquid Al but concentrate within the oxide phase, which enlarge the relative pressure drops and reduce the wetting angles. But Cu addition has the opposite effect as Ti with regards to the equilibrium between alloy and oxide phases. Subsequently, Cu atoms will not enlarge the relative pressure drops and do not improve wetting of Al on B_4C. Here we propose a general wetting principle that an effective alloying element will weaken the bonds within the liquid metal and strength the bonds at the metal/gas interface, alternatively the effective alloying element will have higher partition in the oxide than in the liquid metal phase. Solution thermodynamic models and databases are at handy to predict the chemical equilibrium between alloy and oxide phases, therefore the additive effects for the wetting of metal (or alloy) on oxide (or nonoxide) surfaces can be calculated from solution thermodynamics.

3.4. Prediction of Effective Softening Elements for Liquid Surfaces in B_6Si/Al System. Finally, the wetting of aluminum on solid B_6Si, a potential high strength and low mass MMC, is simulated by using combined solution chemistry and DFT calculations. And new alloy elements (Ti and Zr) to liquid aluminum are proposed that are subject to further experiment study. Here we first start with DFT calculations to study the stability and electronic structure of candidate interfaces. Solution thermodynamic calculations are then conducted to determine the partitions of Ti and Zr between alloy and the Si−B compounds, which complement the DFT study.

The B_6Si has a cubic symmetry (space group: $Pm\bar{3}m$), and the B_3Si has an orthorhombic symmetry (space group: *Imma*). The optimized and experimental lattice parameters of B_6Si, B_3Si, and Al are listed in Table 1. The superlattices of B_6Si/Al and B_3Si/Al are shown in Figure 2. To determine the interfacial formation energies $\Delta H_f(\alpha/\mathrm{Al})$ (α = B_6Si or B_3Si) of superlattice α/Al, we calculated the total energy E(α/Al) for the system consisting of the relaxed supercells of α and Al, and

Table 1. Optimized Parameters of B_3Si, B_6Si and Al[a]

	a_0 (Å)	b_0 (Å)	c_0 (Å)
B_3Si	8.372 (8.392)	12.590 (12.568)	6.223 (6.213)
B_6Si	4.133 (4.130)	4.133	4.133
Al	4.038 (4.050)	4.038	4.038

[a]The values in brackets correspond to the experimental values.

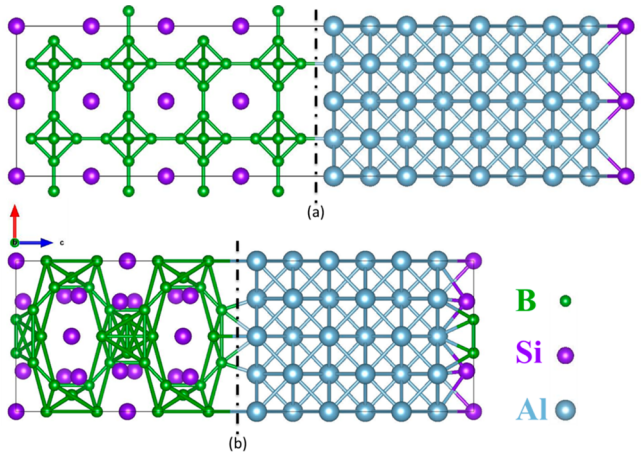

Figure 2. (a) Crystal structures of the (0 0 1) interfaces of B_6Si/Al; (b) crystal structures of the interfaces (0 0 1) of B_3Si/Al.

the total energies E(α) and E(Al) for the individual supercells of α and Al, which the individual supercells is the same with those comprising the superlattices of α/Al. From these quantities, the interfacial formation energy $\Delta H_f(\alpha/\mathrm{Al})$ is defined as

$$\Delta H_f(\alpha/\mathrm{Al}) = [\mathrm{E}(\alpha/\mathrm{Al}) - \mathrm{E}(\alpha) - \mathrm{E}(\mathrm{Al})]/S \quad (8)$$

where S is the area of the interface. The calculated results are listed in Table 2. We find that the interfacial formation energy

Table 2. Calculated Interfacial Formation Energy of B_6Si/Al and B_3Si/Al

α/Al	B_6Si	B_3Si
$\Delta H_f(\alpha/\mathrm{Al})$(eV/Å^2)	−0.14	0.21

of B_6Si/Al is negative ($\Delta H_f(B_6Si/Al)$ = −0.14 eV/Å^2), which means the formation of B_6Si/Al interface is an exothermic process, implying the interface can naturally form. The interfacial formation energy of B_3Si/Al, however, is positive ($\Delta H_f(B_3Si/Al)$ = 0.21 eV/Å^2), which is not chemically favorable.

To calculate the formation energies of B_6Si/Al doped with softening elements, i.e., Cu, Ti, and Zr, we use a softening element substitute one Al atom at the interface. The formation energy $\Delta H_f(B_6Si/Al{:}\beta, q)$ (β = Cu, Ti, and Zr) is defined[47,48] as

$$\Delta H_f(B_6Si/Al{:}\ \beta, q) = \Delta E(B_6Si/Al{:}\ \beta, q) - \mu_\beta + \mu_{Al} + qE_f \quad (9)$$

$$\Delta E(B_6Si/Al{:}\ \beta, q) = E(B_6Si/Al{:}\ \beta, q) - E(B_6Si/Al, q) - \mu^0_\beta + \mu^0_{Al} + qE^0_f \quad (10)$$

where $\Delta E(B_6Si/Al{:}\beta, q)$ is the system containing the softening element in charge state q, $\Delta E(B_6Si/Al, q)$ is the same supercell in the absence of the softening element. μ_i (i = β and Al) is the chemical potential of constituent i referenced to elemental solid or gas with chemical potential μ^0_i. E_f is the electronic Fermi energy of B_6Si/Al:β referenced to Fermi level of B_6Si/Al(E^0_f). The calculated results of B_6Si/Al doped with softening elements are listed in Table 3. We find that all formation energies of B_6Si/Al doped with softening elements are negative,

DOI: 10.1021/am509013m
ACS Appl. Mater. Interfaces 2015, 7, 7576−7583

Table 3. Calculated Formation Energies of B_6Si/Al Doped with Softening Elements (Cu, Ti, and Zr)

β	Cu	Ti	Zr
$\Delta H_f(B_6Si/Al{:}\beta, 0)$ (eV)	−1.04	−1.47	−2.24

implying that these substituting processes are spontaneous without exhausting external energy. Among the three softening elements, the formation energy $\Delta H_f(B_6Si/Al{:}Cu, 0)$ is the highest; however, the formation energy $\Delta H_f(B_6Si/Al{:}Zr, 0)$ is the lowest, which means that the B_6Si/Al doped with Zr is more stable. The reason is that the ability of ionization increases following the order of Cu, Ti, and Zr, meaning that at the interfaces it is easier to form Zr−B than Cu−B and Ti−B bonds. Thus, the softening element Zr is more favorable than the other two.

In Figure 3, we show the projected density of states of the B_6Si/Al superlattice and Cu-, Ti- and Zr-doped superlattice. In

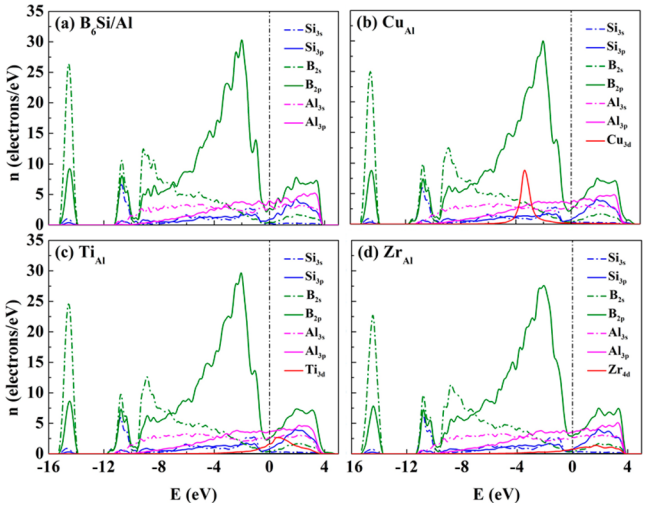

Figure 3. Projected density of states (pDOS) of B_6Si/Al superlattice doped with Cu, Ti, and Zr, respectively. (a) B_6Si/Al superlattice, (b) Cu-doped B_6Si/Al superlattice, (c) Ti-doped B_6Si/Al superlattice, and (d) Zr-doped B_6Si/Al superlattice. The dash-dot line is the Fermi level of the B_6Si/Al superlattice.

Figure 3a, we find that B_{2s}−B_{2p} and Si_{3s}−Si_{3p} have strong s−p hybridization, which is observed from −9 to −12 eV and −14 to −15 eV. The main B_{2p} states are located between 0 and −9 eV, which is coupled with Al_{3s}, Al_{3p}, and Si_{3p} states under the Fermi level. Above the Fermi level, their antibonding states have strong coupling. As we know, the B_{2p} level is at −8.43 eV, Cu_{3d} level is at −20.26 eV, Ti_{3d} level is at −11.05 eV, and Zr_{4d} level is at −8.46 eV.[49] The coupling of Cu_{3d} state and B_{2p} state is weak because the Cu_{3d} level is far below the B_{2p} level. However, the Zr_{4d} state has strong bonding with the B_{2p} state because the Zr_{4d} level is very close to the B_{2p} level. This trend is shown in Figure 3b−3d. In Figure 3b, the Cu_{3d} state is a very local state and far below the Fermi level, which means it has weak bonding with the B_{2p} state. In Figure 3c,d, the antibonding states of Ti_{3d} and Zr_{4d} are pushed above the Fermi level because they have strong coupling with the B_{2p} state. Especially, the Zr_{4d} antibonding state is a nonlocal state, which means its coupling with the B_{2p} state is the strongest among the three softening elements.

In Figure 4, we plot the partial charge density near the Fermi level of B_6Si/Al superlattice and Cu-, Ti-, and Zr-doped

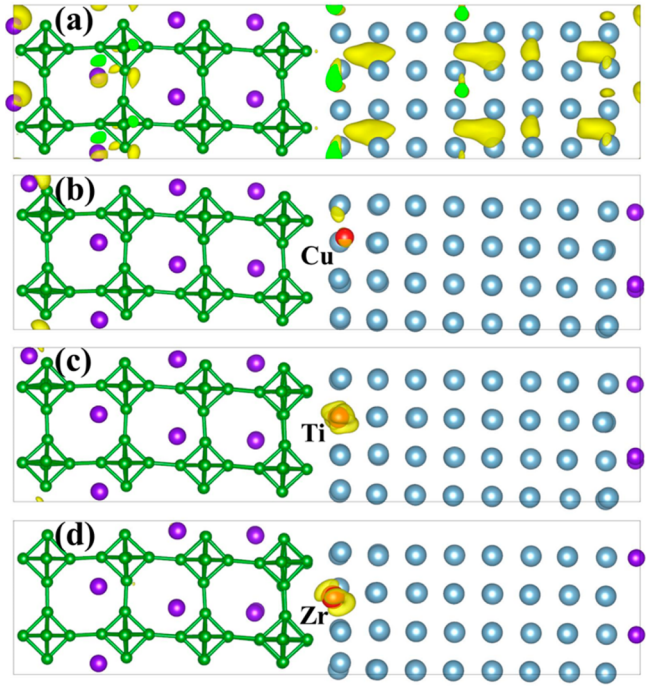

Figure 4. Partial charge density near by the Fermi level of B_6Si/Al superlattice doped with Cu, Ti, and Zr, respectively. (a) B_6Si/Al superlattice, (b) Cu-doped B_6Si/Al superlattice, (c) Ti-doped B_6Si/Al superlattice, and (d) Zr-doped B_6Si/Al superlattice.

superlattice. For the undoped B_6Si/Al superlattice shown in Figure 4a, the main charge density locates in the Al zone. However, the main charge densities of Ti- and Zr-doped superlattice, shown in Figure 4c and 4d, only focus on the Ti and Zr atoms. In Figure 4b, charge density of Cu near the Fermi level is very little because of the lower 3d state of Cu.

Our DFT calculations show that (1) B_6Si/Al is a stable interface and B_3Si/Al is not, (2) Ti and Zr, not Cu, addition promote electron transportation from Al liquid to B_6Si solid at the interfaces. We predict that by a combined Ti and Zr addition, the wetting of Al on B_6Si will be further improved. More experiments will follow in the near future.

For solution thermodynamic calculations, similar to the Al wetting on B_4C, we first calculate the solid oxidation sequence in the B_6Si/Al system by reacting 1 mol of Al and 1 mol of B_6Si with n mol of O_2 at 750 °C, using FactSage software. Al_2O_3 and $(Al_2O_3)_9(B_2O_3)$ start to form, respectively, at $n < 0.001$ and $n = 0.60$, so that the oxidation sequence is first Al^{3+} and then B^{3+}. Therefore, to demonstrate the thermodynamic competition between Zr (or Ti) and Cu additions in the B_6Si/Al system, we simulate their softening effects at the gas/Al(liquid) interfaces by the modified eq 1: an equilibrium calculation at 750 °C of two phases; one liquid alloy (Al + Zr + Cu) plus one liquid oxide (Al_2O_3 + B_2O_3+ Cu_2O+ ZrO_2) as shown below:

$$\mathrm{Al} + \mathrm{Zr} + \mathrm{Cu} + \mathrm{Al_2O_3} + \mathrm{B_2O_3} + \mathrm{Cu_2O} + \mathrm{ZrO_2} = 4.55n^{\mathrm{III}}_{\mathrm{Alloy}} + 3.55n^{\mathrm{III}}_{\mathrm{Oxide}} \quad (11)$$

where the molar fractions of liquid alloy $n^{\mathrm{III}}_{\mathrm{Alloy}}$ are 0.27 Al, 0.66 Cu, and 0.07 Zr, and the molar fractions of liquid oxide $n^{\mathrm{III}}_{\mathrm{Oxide}}$ are 0.25 Al_2O_3, 0.47 ZrO_2, 0.28 B_2O_3, and 6.4×10^{-10} Cu_2O. The calculated partition-configuration-entropy values of Cu and Zr are, respectively, 2.7 and 3.8 J K^{-1} mol^{-1}. Metal Zr and Cu have the highest partitions in the oxide and metal phase,

DOI: 10.1021/am509013m
ACS Appl. Mater. Interfaces 2015, 7, 7576−7583

respectively; in other words, Zr and Cu atoms prefer an oxidized and a reduced electronic state, respectively. This is consistent with the DFT calculations shown in Figure 4, where the partial charge density near by the Fermi level of B_6Si/Al superlattice reaches the highest in the Zr doped and the least in the Cu doped interface. Therefore, the interface is more stable and better wetted with Zr-doping than Cu-doping. Our solution thermodynamic calculation results are consistent with that of DFT calculations.

CONCLUSIONS

A universal wetting principle is established from solution thermodynamic theory and eq 1 to account for the entropy changes and pressure drops at the gas/metal and gas/solid interfaces, and as an example, new additives (Zr and Ti) to improve the wetting of Al on B_6Si are proposed. DFT calculations are applied to confirm the model predictions. Our results show (1) wettability at the metal/gas/substrate interfaces involves not only stable but also metastable chemicals and phases (as in eq 1), which is partially supported by the recent observation on the role of liquid nuclei to the solid−solid transition.[23] And the entropy change during wetting is a dominate factor governing the wetting angles due to the involvement of gas phase. This finding further enforces the current discussion on the role of entropy to phase transition.[27,28] (2) Pressure drops at the gas/pure-metal and gas/pure-substrate interfaces are the main driver for wetting whose temperature dependence can be approximated by using a newly defined thermodynamic parameter, G_{YL} (eq 4). And the Ellingham diagram is handy to calculate G_{YL} and evaluate the changes of oxygen partial pressure with temperature. (3) Additive effects to wetting in Zn galvanizing can be calculated from solution chemistry of the liquid alloy and liquid oxide phases (eqs 1 and 6), which signal their contributions to entropy changes. Additives that prefer to stay in the oxide and away from the alloy lead to improved wettability. (4) Similarly, in the B_4C/Al system, Cu and Ti prefer to stay in alloy and oxide phases, respectively (eqs 1 and 7); therefore, by Ti alloying in aluminum, the wettability is improved. (5) Based on DFT calculations, B_6Si/Al is a stable interface and B_3Si/Al is not. In addition, Ti and Zr, not Cu, addition results in more electron transportation from aluminum liquid to B_6Si, and subsequently leads to reduce wetting angles. This is consistent with the solution thermodynamic calculations (eqs 1 and 11).

Our proposed wetting principle and the specific calculation protocol based on solution thermodynamics (eq 1) that reveals the entropy changes can be applied for the general design of alloy elements to improve the wetting between liquid metal and oxides or boron-containing compounds. Furthermore, it provides a new paradigm for research in catalytic chemistry, heterogeneous nucleation (growth), elastowetting, and cell−substrate interactions.

ASSOCIATED CONTENT

Supporting Information

Optimized structures of DFT models. Table S1: optimized coordinates of B_3Si unit cell. Table S2: optimized coordinates of B_6Si unit cell. Table S3: optimized coordinates of B_3Si (1 × 1 × 2)/Al (2 × 3 × 3) superlattice. Table S4: optimized coordinates of B_6Si (1 × 1 × 4)/Al (1 × 1 × 4) superlattice. Table S5: optimized coordinates of B_6Si (2 × 2 × 4)/Al (2 × 2 × 4) superlattice. This material is available free of charge via the Internet at http://pubs.acs.org/.

AUTHOR INFORMATION

Corresponding Author

*P. Wu. E-mail: wuping@sutd.edu.sg.

Notes

The authors declare no competing financial interest.

REFERENCES

(1) Park, S. J.; Weon, B. M.; Lee, J. S.; Lee, J.; Kim, J.; Je, H. Visualization of Asymmetric Wetting Ridges on Soft Solids with X-ray Microscopy. *Nat. Commun.* **2014**, *5*, 4369.
(2) Duprat, C.; Protiere, S.; Beebe, A. Y.; Stone, H. A. Wetting of Flexible Fibre Arrays. *Nature* **2012**, *482*, 510−513.
(3) Huang, J.; Juszkiewicz, M.; de Jeu, W. H.; Cerda, E.; Emrick, T.; Menon, N.; Russell, T. Capillary Wrinkling of Floating Thin Polymer Films. *Science* **2007**, *317*, 650−653.
(4) Bico, J.; Roman, B.; Moulin, L.; Boudaoud, A. Adhesion: Elastocapillary Coalescence in Wet Hair. *Nature* **2004**, *432*, 690.
(5) Carré, A.; Gastel, J.-C.; Shanahan, M. E. R. Viscoelastic Effects in the Spreading of Liquids. *Nature* **1996**, *379*, 432−434.
(6) Lester, G. R. Contact Angles of Liquids at Deformable Solid Surfaces. *J. Colloid Interface Sci.* **2014**, *16*, 315−326.
(7) Rusanov, A. I. Theory of Wetting of Elastically Deformed Bodies. I. Deformation with a Finite Contact-Angle. *Colloid J.* **1975**, *37*, 614−622.
(8) Shanahan, M. E. R. The Influence of Solid Micro-deformation on Contact Angle Equilibrium. *J. Phys. D: Appl. Phys.* **1987**, *20*, 945−950.
(9) Shanahan, M. E. R.; de Gennes, P. G. In *Adhesion 11*; Allen, K. W., Eds.: Elsevier Applied Science: Amsterdam, 1987; Chapter 5, pp 71−81.
(10) Extrand, C. W.; Kumagai, Y. Contact Angles and Hysteresis on Soft Surfaces. *J. Colloid Interface Sci.* **1996**, *184*, 191−200.
(11) White, L. R. The Contact Angle on an Elastic Substrate. 1. The Role of Disjoining Pressure in the Surface Mechanics. *J. Colloid Interface Sci.* **2003**, *258*, 82−96.
(12) Bonaccurso, E.; Butt, H.-J. Microdrops on Atomic Force Microscope Cantilevers: Evaporation of Water and Spring Constant Calibration. *J. Phys. Chem. B* **2006**, *109*, 253−263.
(13) Py, C.; Reverdy, P.; Doppier, L.; Bico, J.; Roman, B.; Baroud, C. N. Capillary Prigami: Spontaneous Wrapping of a Droplet with an Elastic Sheet. *Phys. Rev. Lett.* **2007**, *98*, 156103.
(14) Pericet-Camara, R.; Auernhammer, G.; Koynov, K.; Lorenzoni, S.; Raiteri, R.; Bonaccurso, E. Solid-Supported Thin Elastomer Films Deformed by Microdrops. *Soft Matter* **2009**, *5*, 3611−3617.
(15) Huang, J.; Davidovitch, B.; Santangelo, C. D.; Russell, T. P.; Menon, N. Smooth Cascade of Wrinkles at the Edge of a Floating Elastic Film. *Phys. Rev. Lett.* **2010**, *105*, 038302.
(16) Jerison, E. R.; Xu, Y.; Wilen, L. A.; Dufresne, E. R. Deformation of an Elastic Substrate by a Three-Phase Contact Line. *Phys. Rev. Lett.* **2011**, *106*, 186103.
(17) Pu, G.; Severtson, S. J. Dependence of Wetting Behavior on the Thickness of Highly Viscoelastic Films. *J. Phys. Chem. C* **2011**, *115*, 18729−18735.
(18) Marchand, A.; Das, S.; Snoeijer, J. H.; Andreotti, B. Contact Angles on a Soft Solid: From Young's Law to Neumann's Law. *Phys. Rev. Lett.* **2012**, *109*, 236101.
(19) Weijs, J. H.; Andreotti, B.; Snoeijer, J. H. Elasto-Capillarity at the Nanoscale: On the Coupling between Elasticity and Surface Energy in Soft Solids. *Soft Matter* **2013**, *9*, 8494.
(20) Style, R. W.; Boltyanskiy, R.; Che, Y.; Wettlaufer, J. S.; Wilen, L. A.; Dufresne, E. R. Universal Deformation of Soft Substrates near a Contact Line and the Direct Measurement of Solid Surface Stresses. *Phys. Rev. Lett.* **2013**, *110*, 066103.
(21) Jin, H. M.; Li, Y.; Liu, H. L.; Wu, P. Study on the Behavior of Additives in Steel Hot-Dip Galvanizing by DFT Calculations. *Chem. Mater.* **2000**, *12*, 1879−1883.
(22) Wu, P.; Jin, H. M.; Liu, H. L. Investigation of Additive Effects on Zn Diffusion in Hot-Dip Galvanizing by DFT Calculations. *Chem. Mater.* **2002**, *14*, 832−837.

DOI: 10.1021/am509013m
ACS Appl. Mater. Interfaces 2015, 7, 7576−7583

(23) Peng, Yi.; Wang, F.; Wang, Z.; Alsayed, A. M.; Zhang, Z.; Yodh, A. G.; Han, Y. Two-Step Nucleation Mechanism in Solid−Solid Phase Transitions. *Nat. Mater.* **2014**, *14*, 101−108.
(24) Naidich, J. V.; Chuvashov, J. N. Wettability and Contact Interaction of Gallium-Containing Melts with Non-metallic Solids. *J. Mater. Sci.* **1983**, *18*, 2071−2080.
(25) Naidich, J. V.; Zhuravljov, V. S.; Frumina, N. I. Wetting of Rare-Earth Element Oxides by Metallic Melts. *J. Mater. Sci.* **1990**, *25*, 1895−1901.
(26) Dezellus, O.; Eustathopoulos, N. Fundamental Issues of Reactive Wetting by Liquid Metals. *J. Mater. Sci.* **2010**, *45*, 4256−4264.
(27) Frenkel, D. Order through Entropy. *Nat. Mater.* **2014**, *14*, 9−12.
(28) Nijs, B. de; Dussi, S.; Smallenburg, F.; Meeldijk, J. D.; Groenendijk, D. J.; Filion, L.; Imhof, A.; Blaaderen, A. van; Dijkstra, M. Entropy-Driven Formation of Large Icosahedral Colloidal Clusters by Spherical Confinement. *Nat. Mater.* **2014**, *14*, 56−60.
(29) Vafaei, S.; Wen, D. Bubble Formation in a Quiescent Pool of Gold Nanoparticle Suspension. *Adv. Colloid Interface Sci.* **2010**, *159*, 72−93.
(30) Pelton, A. D.; Wu, P. Thermodynamic Modeling in Glass-Forming Melts. *J. Non-Cryst. Solids* **1999**, *253*, 178−191.
(31) Lin, S. H.; Hsu, L. Y.; Chou, C. S.; Jhang, J. W.; Wu, P. Carbonization Process of Moso Bamboo (*Phyllostachys pubescens*) Charcoal and its Governing Thermodynamics. *J. Anal. Appl. Pyrolysis* **2014**, *107*, 9−16.
(32) Han, Y. F.; Dai, Y. B.; Wang, J.; Shu, D.; Sun, B. D. First-Principles Calculations on Al/AlB_2 Interfaces. *Appl. Surf. Sci.* **2011**, *257*, 7831−7836.
(33) Zhang, H. L.; Han, Y. F.; Wang, J.; Dai, Y. B.; Sun, B. D. An Ab Initio Molecular Dynamics Study on the Structural and Electronic Properties of AlB_2, TiB_2 and $(Al_xTi_{(1-x)})B_2$ in Al−Ti−B Master Alloys. *J. Alloys Compd.* **2014**, *585*, 529−534.
(34) Yamazaki, K.; Naito, M. Deteriorated Superconductivity of MgB_2 Films due to Al Diffusion from Al_2O_3 Substrates: Thermodynamic Perspective. *Phys. C (Amsterdam, Neth.)* **2013**, *495*, 84−87.
(35) Ellingham Diagrams. http://web.mit.edu/2.813/www/readings/Ellingham_diagrams.pdf.
(36) Bale, C. W.; Belisle, E.; Chartrand, P.; Decterov, S. A.; Eriksson, G.; Hack, K.; Jung, I.-H.; Kang, Y.-B.; Melancon, J.; Pelton, A. D.; Robelin, C.; Petersen, S. FactSage Thermochemical Software and Databases - Recent Developments. *CALPHAD: Comput. Coupling Phase Diagrams Thermochem.* **2009**, *33*, 295−311.
(37) Blöchl, P. E. Projector Augmented-Wave Method. *Phys. Rev. B* **1994**, *50*, 17953−17979.
(38) Perdew, J. P.; Burke, K.; Ernzerhof, M. Generalized Gradient Approximation Made Simple. *Phys. Rev. Lett.* **1996**, *77*, 3865−3868.
(39) Kresse, G.; Furthmuller, J. Efficient Iterative Schemes for Ab Initio Total-Energy Calculations Using a Plane-Wave Basis Set. *Phys. Rev. B* **1996**, *54*, 11169−11186.
(40) Monkhorst, H. J.; Pack, J. D. Special Points for Brillouin-Zone Integrations. *Phys. Rev. B* **1976**, *13*, 5188−5192.
(41) Nogi, K.; Oishi, K.; Ogino, K. Wettability of Solid Oxides by Liquid Pure Metals. *Mater. Trans., JIM* **1989**, *30*, 137−145.
(42) Sebisty, J. J.; Palmer, R. H. *Proceedings of the 7th International Conference on Hot Dip Galvanizing*, Paris, France, June, 1964; Zinc Development Association, Ed.; Pergamon Press: Oxford, U. K., 1967; p 235.
(43) Oh, S. Y.; Cornie, J. A.; Russell, K. C. Wetting of Ceramic Particulates with Liquid Aluminum-Alloys: Part II. Study of Wettability. *Metall. Trans. A* **1989**, *20*, 533−541.
(44) Lai, J.; Zhang, Z.; Chen, X.-G. Effect of Sc, Zr, and Ti on the Interfacial Reactions of the B_4C/Al System. *J. Mater. Sci.* **2011**, *46*, 451−459.
(45) Zheng, J. W.; Nai, S. M. L.; Ng, M.-F.; Wu, P.; Wei, J.; Gupta, M. DFT Study on Nano Structures of Sn/CNT Complex for Potential Li-Ion Battery Application. *J. Phys. Chem. C* **2009**, *113*, 14015−14019.
(46) Zhang, J.; Loh, K. P.; Yang, S. W.; Wu, P. Exohedral Doping of Single-Walled Boron Nitride Nanotube by Atomic Chemisorption. *Appl. Phys. Lett.* **2005**, *87*, 243105.
(47) Zhang, S. B.; Northrup, J. E. Chemical Potential Dependence of Defect Formation Energies in GaAs: Application to Ga Self-Diffusion. *Phys. Rev. Lett.* **1991**, *67*, 2339−2342.
(48) Wei, S.-H. Overcoming the Doping Bottleneck in Semiconductors. *Comput. Mater. Sci.* **2004**, *30*, 337−348.
(49) Harrison, W. A. *Elementary Electronic Structure*, revised ed.; World Scientific Publishing Co. Pte. Ltd.: Singapore, 2004.

DOI: 10.1021/am509013m
ACS Appl. Mater. Interfaces 2015, 7, 7576−7583